

GEMTrans: A General, Echocardiography-based, Multi-Level Transformer Framework for Cardiovascular Diagnosis

Masoud Mokhtari¹, Neda Ahmadi¹, Teresa S. M. Tsang², Purang Abolmaesumi^{1*}, and Renjie Liao¹

¹ Electrical and Computer Engineering, University of British Columbia, Vancouver, BC, Canada

{masoud, nedaahmadi, purang, rjliao}@ece.ubc.ca

² Vancouver General Hospital, Vancouver, BC, Canada
t.tsang@ubc.ca

Abstract. Echocardiography (echo) is an ultrasound imaging modality that is widely used for various cardiovascular diagnosis tasks. Due to inter-observer variability in echo-based diagnosis, which arises from the variability in echo image acquisition and the interpretation of echo images based on clinical experience, vision-based machine learning (ML) methods have gained popularity to act as secondary layers of verification. For such safety-critical applications, it is essential for any proposed ML method to present a level of explainability along with good accuracy. In addition, such methods must be able to process several echo videos obtained from various heart views and the interactions among them to properly produce predictions for a variety of cardiovascular measurements or interpretation tasks. Prior work lacks explainability or is limited in scope by focusing on a single cardiovascular task. To remedy this, we propose a **General, Echo-based, Multi-Level Transformer** (GEMTrans) framework that provides explainability, while simultaneously enabling multi-video training where the inter-play among echo image patches in the same frame, all frames in the same video, and inter-video relationships are captured based on a downstream task. We show the flexibility of our framework by considering two critical tasks including ejection fraction (EF) and aortic stenosis (AS) severity detection. Our model achieves mean absolute errors of 4.15 and 4.84 for single and dual-video EF estimation and an accuracy of 96.5% for AS detection, while providing informative task-specific attention maps and prototypical explainability.

Keywords: Echocardiogram · Transformers · Explainable Models.

1 Introduction and Related Works

Echocardiography (echo) is an ultrasound imaging modality that is widely used to effectively depict the dynamic cardiac anatomy from different standard views

* Corresponding Authors

[23]. Based on the orientation and position of the obtained views with respect to the heart anatomy, different measurements and diagnostic observations can be made by combining information across several views. For instance, Apical Four Chamber (A4C) and Apical Two Chamber (A2C) views can be used to estimate ejection fraction (EF) as they depict the left ventricle (LV), while Parasternal Long Axis (PLAX) and Parasternal Short Axis (PSAX) echo can be used to detect aortic stenosis (AS) due to the visibility of the aortic valve in these views.

Challenges in accurately making echo-based diagnosis have given rise to vision-based machine learning (ML) models for automatic predictions. A number of these works perform segmentation of cardiac chambers; Liu *et al.* [14] perform LV segmentation using feature pyramids and a segmentation coherency network, while Cheng *et al.* [3] and Thomas *et al.* [24] use contrastive learning and GNNs for the same purpose, respectively. Some others introduce ML frameworks for echo view classification [8,10] or detecting important phases (e.g. end-systole (ES) and end-diastole (ED)) in a cardiac cycle [7]. Other bodies of work focus on making disease prediction from input echo. For instance, Duffy *et al.* [6] perform landmark detection to predict LV hypertrophy, while Roshanitabrizi *et al.* [20] predict rheumatic heart disease from Doppler echo using an ensemble of transformers and convolutional neural networks. In this paper, however, we focus on ejection fraction (EF) estimation and aortic stenosis severity (AS) detection as two example applications to showcase the generality of our framework and enable its comparison to prior works in a tractable manner. Therefore, in the following two paragraphs, we give a brief introduction to EF, AS and prior automatic detection works specific to these tasks.

EF is a ratio that indicates the volume of blood pumped by the heart and is an important indicator of heart function. The clinical procedure to estimating this ratio involves finding the ES and ED frames in echo cine series (videos) and tracing the LV on these frames. A high level of inter-observer variability of 7.6% to 13.9% has been reported in clinical EF estimates [18]. Due to this, various ML models have been proposed to automatically estimate EF and act as secondary layers of verification. More specifically, Eseh *et al.* [13] propose a Bayesian network that produces uncertainty along with EF predictions, while Reynaud *et al.* [19] use BERT [4] to capture frame-to-frame relationships. Recently, Mokhtari *et al.* [16] provide explainability in their framework by learning a graph structure among frames of an echo.

The other cardiovascular task we consider is the detection of AS, which is a condition in which the aortic valve becomes calcified and narrowed, and is typically detected using spectral Doppler measurements [21,17]. High inter-observer variability, limited access to expert cardiac physicians, and the unavailability of spectral Doppler in many point-of-care ultrasound devices are challenges that can be addressed through the use of automatic AS detection models. For example, Huang *et al.* [11,12] predict the severity of AS from single echo images, while Ginsberg *et al.* [9] adopt a multitask training scheme.

Our framework is distinguished from prior echo-based works on multiple fronts. First, to the best of our knowledge, our model is the first to produce

attention maps on the patch, frame and video levels for echo data, while allowing multiple videos to be processed simultaneously as shown in Fig. 1. Second, unlike prior works that are proposed for a single cardiovascular task, our framework is general and can be modified for a variety of echo-based metrics. More concretely, the versatility of our framework comes from its multi-level attention mechanism. For example, for EF, temporal attention between the echo frames is critical to capture the change in the volume of the LV, while for AS, spatial attention to the valve area is essential, which is evident by how the model is trained to adapt its learned attention to outperform all prior works. Lastly, we provide patch and frame-level, attention-guided prototypical explainability.

Our contributions are summarized below:

- We propose GEMTrans, a general, transformer-based, multi-level ML framework for vision-based medical predictions on echo cine series (videos).
- We show that the task-specific attention learned by the model is effective in highlighting the important patches and frames of an input video, which allows the model to achieve a mean absolute error of 4.49 on two EF datasets, and a detection accuracy score of 96.5% on an AS dataset.
- We demonstrate how prototypical learning can be easily incorporated into the framework for added multi-layer explainability.

2 Method

2.1 Problem Statement

The input data for both EF and AS tasks compose of one or multiple B-mode echo videos denoted by $X \in \mathbb{R}^{K \times T \times H \times W}$, where K is the number of videos per sample, T is the number of frames per video, and H and W are the height and width of each grey-scale image frame. For **EF Estimation**, we consider both the single video (A4C) and the dual video (A2C and A4C) settings corresponding to $K = 1$ and $K = 2$, respectively. Our datasets consist of triplets $\{x_{\text{ef}}^i, y_{\text{ef}}^i, y_{\text{seg}}^i\}$, where $i \in [1, \dots, n]$ is the sample number. $y_{\text{ef}}^i \in [0, 1]$ is the ground truth EF value, $y_{\text{seg}}^i \in \{0, 1\}^{H \times W}$ is the binary LV segmentation mask, and $x^i \in \mathbb{R}^{K \times T \times H \times W}$ are the input videos defined previously. The goal is to learn an EF estimation function $f_{\text{ef}} : \mathbb{R}^{K \times T \times H \times W} \mapsto \mathbb{R}$. For **AS Classification**, we consider the dual-video setting (PLAX and PSAX). Here, our dataset $D_{\text{as}} = \{X_{\text{as}}, Y_{\text{as}}\}$ consists of pairs $\{x_{\text{as}}^i, y_{\text{as}}^i\}$, where x_{as}^i are the input videos and $y_{\text{as}}^i \in \{0, 1\}^4$ is a one-hot label indicating healthy, mild, moderate and severe AS cases. Our goal is to learn $f_{\text{as}} : \mathbb{R}^{2 \times T \times H \times W} \mapsto \mathbb{R}^4$ that produces a probability over AS severity classes.

2.2 Multi-Level Transformer Network

As shown in Fig. 1, we employ a three-level transformer network, where the levels are tasked with patch-wise, frame-wise and video-wise attention, respectively.

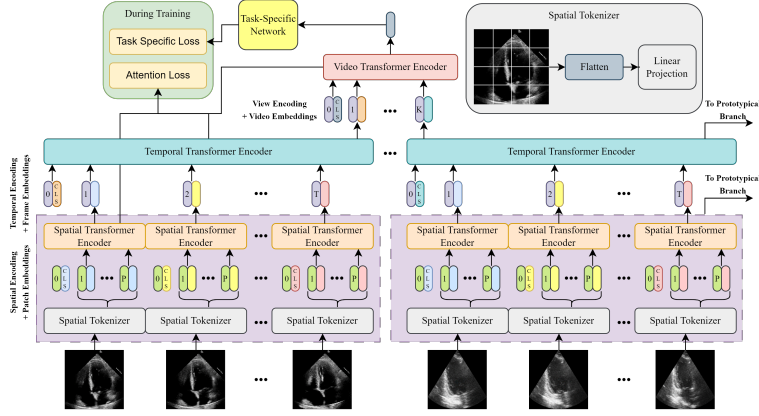


Fig. 1: **GEMTrans Overview** - The multi-level transformer network processes one or multiple echo videos and is composed of three main components. *Spatial Transformer Encoder (STE)* produces attention among patches in the same image frame, while *Temporal Transformer Encoder (TTE)* captures the temporal dependencies among the frames of each video. Lastly, *Video Transformer Encoder (VTE)* produces an embedding summarizing all available data for a patient by processing the learned embedding of each video. Different downstream tasks can then be performed using this final learned embedding. During training, both the final prediction and the attention learned by different layers of the framework can be supervised (not all connections are shown for cleaner visualization).

Spatial Transformer Encoder (STE) captures the attention among patches within a certain frame and follows ViT’s [5] architecture. As shown in Eqs. (1) and (2), the Spatial Tokenizer (ST) first divides the image into non-overlapping $p \times p$ sized patches before flattening and linearly projecting each patch:

$$\hat{x}_{k,t} = [\hat{x}_{k,t,1}, \hat{x}_{k,t,2}, \dots, \hat{x}_{k,t,HW/p^2}] = f_{\text{patch}}(x_{k,t}, p); \quad (1)$$

$$x'_{k,t} = [x'_{k,t,1}, x'_{k,t,2}, \dots, x'_{k,t,HW/p^2}] = f_{\text{lin}}(\text{flatten}(\hat{x}_{k,t})), \quad (2)$$

where p is the patch size, $k \in [1, \dots, K]$ is the video number, $t \in [1, \dots, T]$ is the frame number, $f_{\text{patches}} : \mathbb{R}^{H \times W} \mapsto \mathbb{R}^{HW/p^2 \times p \times p}$ splits the image into equally-sized patches, and $f_{\text{lin}} : \mathbb{R}^{p^2} \mapsto \mathbb{R}^d$ is a linear projection function that maps the flattened patches into d -dimensional embeddings. The obtained tokens from the ST are then fed into a transformer network [25] as illustrated in Eqs. (3) to (6):

$$h_{k,t}^0 = [\text{cls}_{\text{spatial}}; x'_{k,t}] + E_{\text{pos}}; \quad (3)$$

$$h_{k,t}^l = \text{MHA}(\text{LN}(h_{k,t}^{l-1})) + h_{k,t}^{l-1}, \quad l \in [1, \dots, L]; \quad (4)$$

$$h_{k,t}^l = \text{MLP}(\text{LN}(h_{k,t}^l)) + h_{k,t}^l, \quad l \in [1, \dots, L]; \quad (5)$$

$$z_{k,t} = \text{LN}(h_{k,t}^L), \quad (6)$$

where $\text{cls}_{\text{spatial}} \in \mathbb{R}^d$ is a token similar to the $[class]$ token introduced by Devlin *et al.* [4], $E_{\text{pos}} \in \mathbb{R}^d$ is a learnable positional embedding, MHA is a multi-head attention network [25], LN is the LayerNorm operation, and MLP is a multi-layer perceptron. The obtained result $z_{k,t} \in \mathbb{R}^d$ can be regarded as an embedding summarizing the t_{th} frame in the k_{th} video for a sample.

Temporal Transformer Encoder (TTE) accepts as input the learned embeddings of the STE for each video $z_{k,1\dots T}$ and performs similar operations outlined in Eqs. (3) to (6) to generate a single embedding $v_k \in \mathbb{R}^d$ representing the whole video from the k_{th} view. **Video Transformer Encoder (VTE)** is the same as TTE with the difference that each input token $v_k \in \mathbb{R}^d$ is a representation for a complete video from a certain view. The output of VTE is an embedding $u^i \in \mathbb{R}^d$ summarizing the data available for patient i . This learned embedding can be used for various downstream tasks as described in Sec. 2.5.

2.3 Attention Supervision

For EF, the ED/ES frame locations and their LV segmentation are available. This intermediary information can be used to supervise the learned attention of the transformer. Therefore, inspired by Stacey *et al.* [22], we supervise the last-layer attention that the cls token allocates to other tokens. More specifically, for spatial attention, we penalize the model for giving attention to the region outside the LV, while for temporal dimension, we encourage the model to give more attention to the ED/ES frames. More formally, we define $\text{ATTN}_{\text{cls}}^{\text{spatial}} \in [0, 1]^{HW/p^2}$ and $\text{ATTN}_{\text{cls}}^{\text{temporal}} \in [0, 1]^T$ to be the L_{th} -layer, softmax-normalized spatial and temporal attention learned by the MHA module (see Eq. (4)) of STE and TTE, respectively. The attention loss is defined as

$$y'_{\text{seg}} = \text{OR}(y_{\text{seg}}^{\text{ed}}, y_{\text{seg}}^{\text{es}}); \quad (7)$$

$$L_{\text{attn, s}}^{\text{spatial}} = \begin{cases} (\text{ATTN}_{\text{cls, s}}^{\text{spatial}} - 0)^2, & \text{if } y'_{\text{seg, s}} = 0 \text{ (outside LV)} \\ 0, & \text{otherwise;} \end{cases} \quad (8)$$

$$L_{\text{attn, t}}^{\text{temporal}} = \begin{cases} (\text{ATTN}_{\text{cls, s}}^{\text{temporal}} - 1)^2, & \text{if } t \in [\text{ED, ES}] \\ 0, & \text{otherwise;} \end{cases} \quad (9)$$

$$L_{\text{attn}} = \lambda_{\text{temporal}} \sum_{t=1}^T L_{\text{attn, t}}^{\text{temporal}} + \lambda_{\text{spatial}} \sum_{s=1}^{HW/p^2} L_{\text{attn, s}}^{\text{spatial}}, \quad (10)$$

where $y_{\text{seg}}^{\text{ed}}, y_{\text{seg}}^{\text{es}} \in \{0, 1\}^{HW/p^2}$ are the coarsened versions (to match patch size) of y_{seg} at the ED and ES locations, OR is the bit-wise logical *or* function, ed/es indicate the ED/ES temporal frame indices, and $\lambda_{\text{temporal}}, \lambda_{\text{spatial}} \in [0, 1]$ control the effect of spatial and temporal losses on the overall attention loss. A figure is provided in the supp. material for further clarification.

2.4 Prototypical Learning

Prototypical learning provides explainability by presenting training examples (prototypes) as the reasoning for choosing a certain prediction. As an example,

in the context of AS, patch-level prototypes can indicate the most important patches in the training frames that correspond to different AS cases. Due to the multi-layer nature of our framework and inspired by Xue *et al.* [26], we can expand this idea and use our learned attention to filter out uninformative details prior to learning patch and frame-level prototypes. As shown in Fig. 1, the STE and TTE’s attention information are used in prototypical branches to learn these prototypes. It must be noted that we are not using prototypical learning to improve performance, but rather to provide added explainability. For this reason, prototypes are obtained in a post-processing step using the pretrained transformer framework. *Prototypical networks are provided in the supp. material.*

2.5 Downstream Tasks and Optimization

The output embedding of VTE denoted by $u \in \mathbb{R}^{n \times d}$ can be used for various downstream tasks. We use Eq. (11) to generate predictions for EF and use an L2 loss between \hat{y}_{ef} and y_{ef}^i for optimization denoted by L_{ef} . For AS severity classification, Eq. (12) is used to generate predictions and a cross-entropy loss is used for optimization shown as L_{as} :

$$\hat{y}_{\text{ef}} = \sigma(\text{MLP}(u)) \quad \hat{y}_{\text{ef}} \in \mathbb{R}^{n \times 1}; \quad (11)$$

$$\hat{y}_{\text{as}} = \text{softmax}(\text{MLP}(u)) \quad \hat{y}_{\text{as}} \in \mathbb{R}^{n \times 4}; \quad (12)$$

$$L_{\text{overall}} = L_{\text{ef or as}} + L_{\text{attn}}, \quad (13)$$

where σ is the Sigmoid function. Our overall loss function is shown in Eq. (13).

3 Experiments

3.1 Implementation

Our code-base, pre-trained model weights and the corresponding configuration files are provided at <https://github.com/DSL-Lab/gemtrans>. All models were trained on four 32 GB NVIDIA Tesla V100 GPUs, where the hyper-parameters are found using Weights & Biases random sweep [2]. Lastly, we use the ViT network from [15] pre-trained on ImageNet-21K for the STE module.

3.2 Datasets

We compare our model’s performance to prior works on three datasets. In summary, for the single-video case, we use the EchoNet Dynamic dataset that consists of 10,030 AP4 echo videos obtained at Stanford University Hospital [18] with a training/validation/test (TVT) split of 7,465, 1,288 and 1,277. For the dual-video setting, we use a private dataset of 5,143 pairs of AP2/AP4 videos with a TVT split of 3,649, 731, 763. For the AS severity detection task, we use a private dataset of PLAX/PSAX pairs with a balanced number of healthy,

mild, moderate and severe AS cases and a TVT of 1, 875, 257, and 258. For all datasets, the frames are resized to 224×224 . Our use of this private dataset is approved by the University of British Columbia Research Ethics Board, with an approval number H20-00365.

3.3 Results

Quantitative Results: In Tables 1 and 2, we show that our model outperforms all previous work in EF estimation and AS detection. For EF, we use the mean absolute error (MAE) between the ground truth and the predicted EF values, and R^2 correlation score. For AS, we use an accuracy metric for four-class AS severity prediction and binary detection of AS. The results show the flexibility of our model to be adapted for various echo-based tasks while achieving high levels of performance. **Qualitative Results:** In addition to having the superior quantitative performance, we show that our model provides explainability through its task-specific learned attention (Fig. 2a) and the learned prototypes (Fig. 2b). *More results are shown in the supp. material.* **Ablation Study:** We show the effectiveness of our design choices in Table 3, where we use EF estimation for the EchoNet Dynamic dataset as our test-bed. It is evident that our attention loss described in Sec. 2.3 is effective for EF when intermediary labels are available, while it is necessary to use a pre-trained ViT as the size of medical datasets in our experiments are not sufficiently large to build good inductive bias.

Table 1: **Quantitative results for EF** on the test set - LV Biplane dataset results for models not supporting multi-video training are indicated by ”-”. MAE is the Mean Absolute Error and R^2 indicates variance captured by the model.

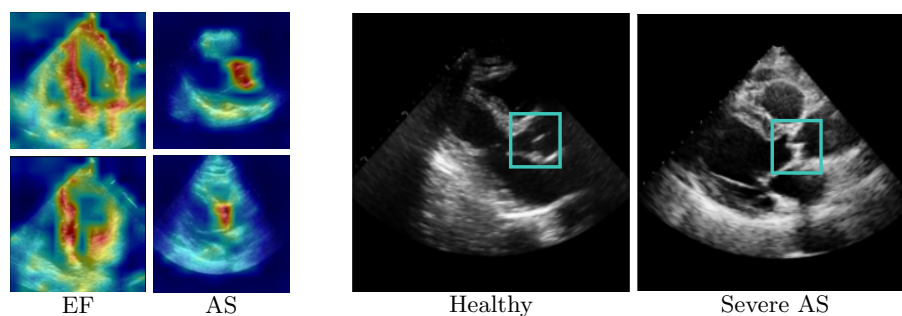
Model	EchoNet Dynamic		LV Biplane	
	MAE [mm] ↓	R^2 Score ↑	MAE [mm] ↓	R^2 Score ↑
Ouyang <i>et al.</i> [18]	7.35	0.40	-	-
Reynaud <i>et al.</i> [19]	5.95	0.52	-	-
Esfeh <i>et al.</i> [13]	4.46	0.75	-	-
Thomas <i>et al.</i> [24]	4.23	0.79	-	-
Mokhtari <i>et al.</i> [16]	4.45	0.76	5.12	0.68
Ours	4.15	0.79	4.84	0.72

4 Conclusions and Future Work

In this paper, we introduced a multi-layer, transformer-based framework suitable for processing echo videos and showed superior performance to prior works

Table 2: **Quantitative results for AS** on the test set - *Severity* is a four-class classification task, while *Detection* involves the binary detection of AS.

Model	Accuracy [%] \uparrow	
	Severity	Detection
Huang <i>et al.</i> [12]	73.7	94.1
Bertasius <i>et al.</i> [1]	75.3	94.8
Ginsberg <i>et al.</i> [9]	74.4	94.2
Ours	76.2	96.5



(a) **Learned Patch-Level Attention** - We visualize the learned attention of STE, where for EF, the model is focusing on the walls of the LV, while for AS, the model learns to attend to the valve area, which is clinically correct.

(b) **Learned Patch-Level Prototypes** - Learned prototypes use STE’s attention to properly focus on the valve area for a healthy and severe AS case. We can see that in the healthy case, the aortic valve is thin and not calcified. However, in the severe case, the calcification of aortic valve is apparent (i.e. the valve appears bright in the image). *Frame-level and EF prototypes presented in supp. material.*

Fig. 2: **Explainability** through learned attention and prototypes.

Table 3: **Ablation study** on the validation set of EchoNet Dynamic - We see that both spatial and temporal attention supervision are effective for EF estimation, while the model does not converge without pretraining the ViT. MAE is the Mean Absolute Error and R^2 indicates variance captured by the model.

Model	MAE [mm] \downarrow	R^2 Score \uparrow
No Spatial Attn. Sup.	4.42	0.77
No Temporal Attn. Sup.	4.54	0.76
No ViT Pretraining	5.61	0.45
Ours	4.11	0.80

on two challenging tasks while providing explainability through the use of prototypes and learned attention of the model. Future work will include training a large multi-task model with a comprehensive echo dataset that can be disseminated to the community for a variety of clinical applications.

References

1. Bertasius, G., Wang, H., Torresani, L.: Is space-time attention all you need for video understanding? In: Meila, M., Zhang, T. (eds.) Proceedings of the 38th International Conference on Machine Learning. Proceedings of Machine Learning Research, vol. 139, pp. 813–824. PMLR (2021) [8](#)
2. Biewald, L.: Experiment tracking with weights and biases (2020) [6](#)
3. Cheng, L.H., Sun, X., van der Geest, R.J.: Contrastive learning for echocardiographic view integration. In: Medical Image Computing and Computer Assisted Intervention. pp. 340–349. Springer Nature Switzerland, Cham (2022) [2](#)
4. Devlin, J., Chang, M.W., Lee, K., Toutanova, K.: Bert: Pre-training of deep bidirectional transformers for language understanding. (2019) [2](#), [5](#)
5. Dosovitskiy, A., Beyer, L., Kolesnikov, A., Weissenborn, D., Zhai, X., Unterthiner, T., Dehghani, M., Minderer, M., Heigold, G., Gelly, S., Uszkoreit, J., Houslyby, N.: An image is worth 16x16 words: Transformers for image recognition at scale. In: International Conference on Learning Representations (2021) [4](#)
6. Duffy, G., Cheng, P.P., Yuan, N., He, B., Kwan, A.C., Shun-Shin, M.J., Alexander, K.M., Ebinger, J., Lungren, M.P., Rader, F., Liang, D.H., Schnittger, I., Ashley, E.A., Zou, J.Y., Patel, J., Wittles, R., Cheng, S., Ouyang, D.: High-Throughput Precision Phenotyping of Left Ventricular Hypertrophy With Cardiovascular Deep Learning. *JAMA Cardiology* **7**(4), 386–395 (2022) [2](#)
7. Fiorito, A.M., Østvik, A., Smistad, E., Leclerc, S., Bernard, O., Lovstakken, L.: Detection of cardiac events in echocardiography using 3d convolutional recurrent neural networks. In: IEEE International Ultrasonics Symposium. pp. 1–4 (2018) [2](#)
8. Gao, X., Li, W., Loomes, M., Wang, L.: A fused deep learning architecture for view-point classification of echocardiography. *Information Fusion* **36**, 103–113 (2017) [2](#)
9. Ginsberg, T., Tal, R.e., Tsang, M., Macdonald, C., Dezaki, F.T., van der Kuur, J., Luong, C., Abolmaesumi, P., Tsang, T.: Deep video networks for automatic assessment of aortic stenosis in echocardiography. In: Noble, J.A., Aylward, S., Grimwood, A., Min, Z., Lee, S.L., Hu, Y. (eds.) Simplifying Medical Ultrasound. pp. 202–210. Springer International Publishing, Cham (2021) [2](#), [8](#)
10. Gu, A.N., Luong, C., Jafari, M.H., Van Woudenberg, N., Girgis, H., Abolmaesumi, P., Tsang, T.: Efficient echocardiogram view classification with sampling-free uncertainty estimation. In: Noble, J.A., Aylward, S., Grimwood, A., Min, Z., Lee, S.L., Hu, Y. (eds.) Simplifying Medical Ultrasound. pp. 139–148. Springer International Publishing, Cham (2021) [2](#)
11. Huang, Z., Long, G., Wessler, B., Hughes, M.C.: A new semi-supervised learning benchmark for classifying view and diagnosing aortic stenosis from echocardiograms. In: Proceedings of the 6th Machine Learning for Healthcare Conference (2021) [2](#)
12. Huang, Z., Long, G., Wessler, B., Hughes, M.C.: Tmed 2: A dataset for semi-supervised classification of echocardiograms (2022) [2](#), [8](#)
13. Kazemi Esfeh, M.M., Luong, C., Behnami, D., Tsang, T., Abolmaesumi, P.: A deep bayesian video analysis framework: Towards a more robust estimation of ejection

- fraction. In: Martel, A.L., Abolmaesumi, P., Stoyanov, D., Mateus, D., Zuluaga, M.A., Zhou, S.K., Racoceanu, D., Joskowicz, L. (eds.) *Medical Image Computing and Computer Assisted Intervention*. pp. 582–590. Springer International Publishing, Cham (2020) [2](#), [7](#)
14. Liu, F., Wang, K., Liu, D., Yang, X., Tian, J.: Deep pyramid local attention neural network for cardiac structure segmentation in two-dimensional echocardiography. *Medical Image Analysis* **67**, 101873 (2021) [2](#)
 15. Melas-Kyriazi, L.: Vit pytorch (2020), <https://github.com/lukemelas/PyTorch-Pretrained-ViT> [6](#)
 16. Mokhtari, M., Tsang, T., Abolmaesumi, P., Liao, R.: Echognn: Explainable ejection fraction estimation with graph neural networks. In: Wang, L., Dou, Q., Fletcher, P.T., Speidel, S., Li, S. (eds.) *Medical Image Computing and Computer Assisted Intervention*. pp. 360–369. Springer Nature Switzerland, Cham (2022) [2](#), [7](#)
 17. Otto, C.M., Nishimura, R.A., Bonow, R.O., Carabello, B.A., Erwin, J.P., Gentile, F., Jneid, H., Krieger, E.V., Mack, M., McLeod, C., O’Gara, P.T., Rigolin, V.H., Sundt, T.M., Thompson, A., Toly, C.: 2020 acc/aha guideline for the management of patients with valvular heart disease: Executive summary. *Journal of the American College of Cardiology* **77**(4), 450–500 (2021) [2](#)
 18. Ouyang, D., He, B., Ghorbani, A., Yuan, N., Ebinger, J.E., Langlotz, C., Heidenreich, P.A., Harrington, R.A., Liang, D.H., Ashley, E.A., Zou, J.Y.: Video-based ai for beat-to-beat assessment of cardiac function. *Nature* **580**, 252–256 (2020) [2](#), [6](#), [7](#)
 19. Reynaud, H., Vlontzos, A., Hou, B., Beqiri, A., Leeson, P., Kainz, B.: Ultrasound video transformers for cardiac ejection fraction estimation. In: *Medical Image Computing and Computer Assisted Intervention*. pp. 495–505. Springer International Publishing, Cham (2021) [2](#), [7](#)
 20. Roshanibrizi, P., Roth, H.R., Tompsett, A., Paulli, A.R., Brown, K., Rwebember, J., Okello, E., Beaton, A., Sable, C., Linguraru, M.G.: Ensembled prediction of rheumatic heart disease from ungated doppler echocardiography acquired in low-resource settings. In: *Medical Image Computing and Computer Assisted Intervention*. pp. 602–612. Springer Nature Switzerland, Cham (2022) [2](#)
 21. Spitzer, E., Hahn, R.T., Pibarot, P., de Vries, T., Bax, J.J., Leon, M.B., Mieghem, N.M.V.: Aortic stenosis and heart failure: Disease ascertainment and statistical considerations for clinical trials. *Cardiac Failure Review* **5**, 99 – 105 (2019) [2](#)
 22. Stacey, J., Belinkov, Y., Rei, M.: Supervising model attention with human explanations for robust natural language inference. *Proceedings of the AAAI Conference on Artificial Intelligence* **36**(10), 11349–11357 (2022) [5](#)
 23. Suetens, P.: *Fundamentals of Medical Imaging*. Cambridge University Press, 2 edn. (2009) [2](#)
 24. Thomas, S., Gilbert, A., Ben-Yosef, G.: Light-weight spatio-temporal graphs for segmentation and ejection fraction prediction in cardiac ultrasound. In: Wang, L., Dou, Q., Fletcher, P.T., Speidel, S., Li, S. (eds.) *Medical Image Computing and Computer Assisted Intervention*. pp. 380–390. Springer Nature Switzerland, Cham (2022) [2](#), [7](#)
 25. Vaswani, A., Shazeer, N., Parmar, N., Uszkoreit, J., Jones, L., Gomez, A.N., Kaiser, L.u., Polosukhin, I.: Attention is all you need. In: Guyon, I., Luxburg, U.V., Bengio, S., Wallach, H., Fergus, R., Vishwanathan, S., Garnett, R. (eds.) *Advances in Neural Information Processing Systems*. vol. 30. Curran Associates (2017) [4](#), [5](#)
 26. Xue, M., Huang, Q., Zhang, H., Cheng, L., Song, J., hui Wu, M., Song, M.: Protopformer: Concentrating on prototypical parts in vision transformers for interpretable image recognition. *ArXiv* (2022) [6](#)

Supplementary Material

Masoud Mokhtari et al.

Electrical and Computer Engineering, University of British Columbia, Vancouver,
BC, Canada

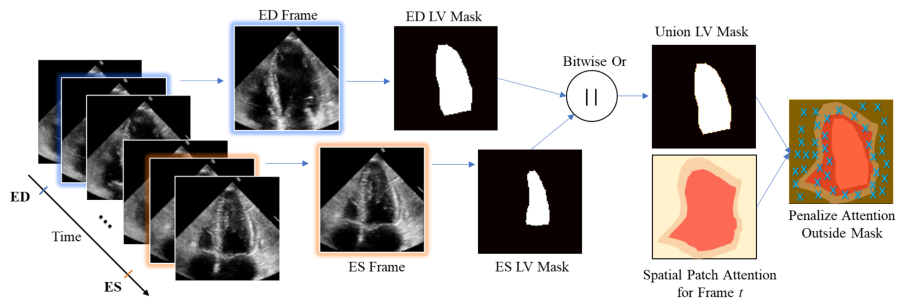


Fig. 1: **Attention Supervision** - For EF, the spatial attention is penalized if attention is given outside the union of the LV mask for ED and ES. The temporal attention is also encouraged to give more attention to ED/ES locations.

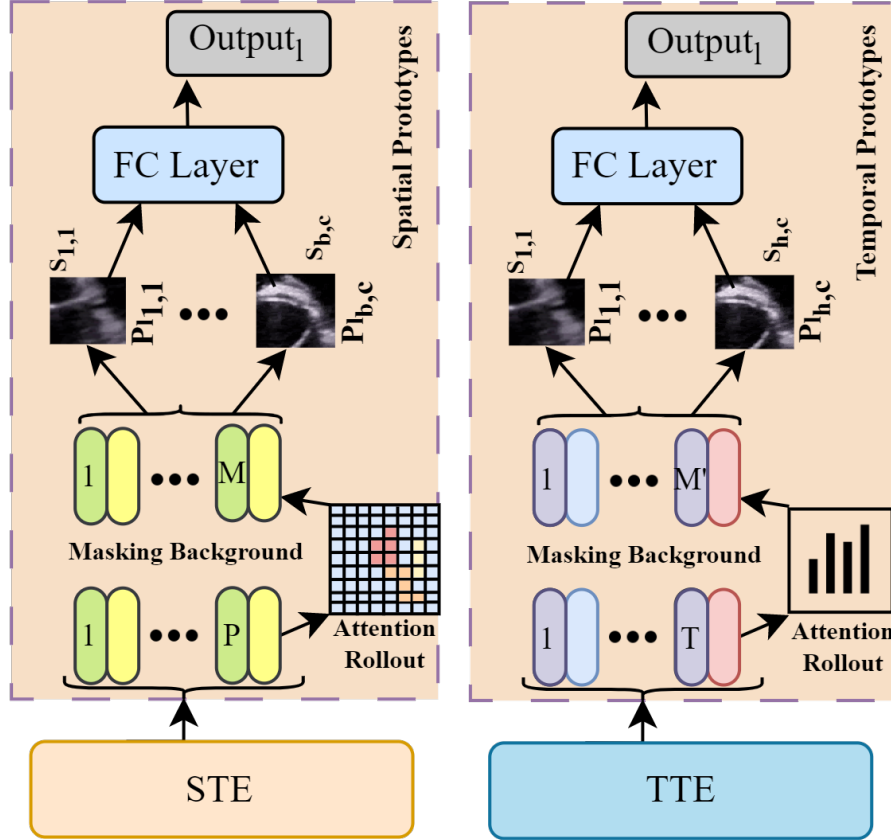


Fig. 2: **Prototypical Network** - For spatial (patch-level) prototypes, the learned local tokens $z_{k,t} \in \mathbb{R}^{HW/p^2 \times d}$ of STE are used. M patches with the highest attention are included and the rest are eliminated. Remaining patches are compared with B learnable prototypes for each class $P_l = \{p_{l,b,c}\}_{b=1,c=1}^{B_l,C} \in \mathbb{R}^d$ producing a similarity vector $s \in \mathbb{R}^{B \times C}$ where C is the number of classes. Fully connected layers map these similarity scores to the output. For temporal prototypes, the frame-level tokens $z'_{k,t}$ of TTE are given as input. M' frames with high temporal attention are kept and compared with H learnable prototypes and the similarity scores produce the output.

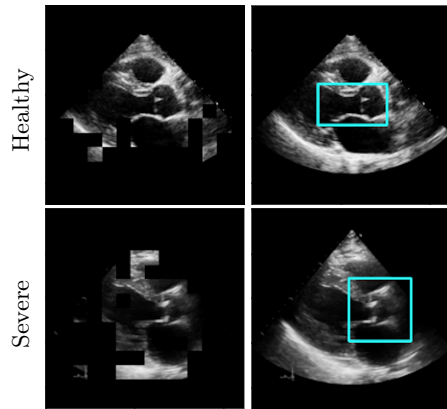


Fig. 3: **Additional Patch-Level Prototypes for AS** - Left figures demonstrate discarded patches based on the acquired attention of STE. Patches with low attention are eliminated. The right figures display the areas that correspond to the learned prototypes. In both the healthy and severe cases, there is a notable emphasis on the aortic valve.

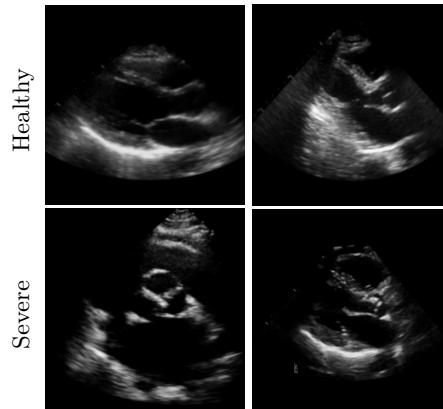


Fig. 4: **Frame-Level Prototypes for AS** - Two instances of frame-level prototypes are visualized for healthy and severe AS. The majority of frame-level prototypes are indicative of end-systole and mid-systole stage of the heart cycle in which the restriction of valve's motion and detection of the aortic valve's calcification is easier.

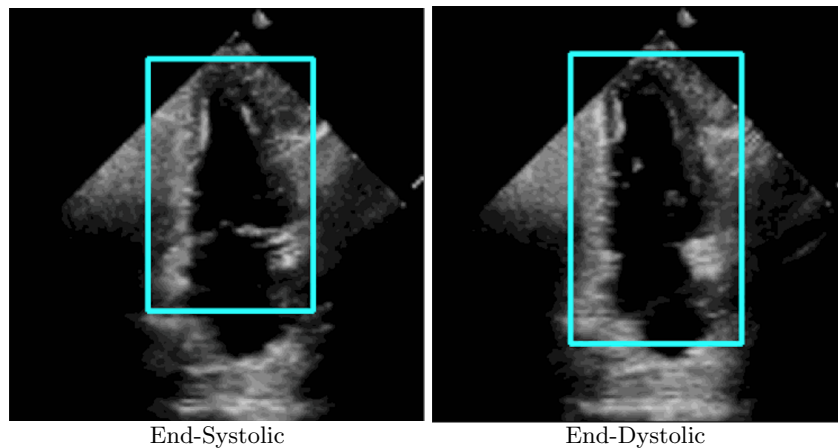


Fig. 5: **Patch-Level Prototypes for EF** - This figure visualizes the patch-level prototypes that represent the LV in ES and ED frames. This suggests that these frames are the most significant in contributing to the final estimation of EF, which is clinically correct since the ratio of the volume of blood in ED and ES are used to find EF.